Biologia (2025) 80:1513–1530
https://doi.org/10.1007/s11756-025-01916-5

ORIGINAL ARTICLE

Computational drug repurposing reveals potential alanine racemase inhibitors for combating drug-resistant tuberculosis

Keerthika LakshmanaPerumal[2] · Umashankar Vetrivel[1]

Received: 10 January 2025 / Accepted: 26 February 2025 / Published online: 24 March 2025
© Plant Science and Biodiversity Centre, Slovak Academy of Sciences (SAS), Institute of Zoology, Slovak Academy of Sciences (SAS), Institute of Molecular Biology, Slovak Academy of Sciences (SAS) 2025

Abstract

The management of tuberculosis (TB) poses a significant challenge, particularly in low- to middle-income regions, due to its high mortality rate and severity. Given the paramount importance of maintaining the structural integrity of the bacterial cell wall, alanine racemase emerges as a critical therapeutic target due to its key role in the peptidoglycan pathway and its unique absence in humans. However, the imperative to discover novel inhibitors targeting this pathway is underscored by the rise of drug-resistant TB strains. In this study, we employed a computational drug repurposing approach to predict potential alanine racemase inhibitors by screening FDA-listed drugs cataloged in DrugBank 5.1.9. Additionally, docking studies used cycloserine, a known alanine racemase inhibitor, as a reference compound. The prioritization of a potent inhibitor relied on multiple criteria, including binding affinity, intermolecular interaction patterns, MMGBSA analysis, ΔG calculations, ADMET properties, and molecular dynamics simulations to evaluate the protein-drug complex stability. Our comprehensive analysis identified three compounds (DB00712, DB09064, and DB05015) as potential hits, successfully passing all prioritization processes. However, DB09064 exhibited the most promising attributes among these candidates, demonstrating enhanced complex stability, binding affinity (-8.5 kcal/mol), and significant intermolecular interactions. Furthermore, its interaction pattern and Protein-Drug complex Root Mean Square Deviation (RMSD) trajectory closely resembled cycloserine, indicating its potential in targeting alanine racemase. Therefore, DB09064 (Ciprofibrate) is predicted as a highly potential hit. With further lead optimization and experimental validation to mitigate off-target effects, it could emerge as a novel alanine racemase inhibitor, offering potential implications for combating drug-resistant TB.

Keywords Alanine racemase · Drug repurposing · *Mycobacterium tuberculosis* · Peptidoglycan pathway · Inhibitors

Abbreviations

TB	Tuberculosis
FDA	Food and Drug Administration
MMGBSA	Molecular mechanics with generalized born and surface
ADMET	Absorption, distribution, metabolism, excretion and toxicity
DB	DrugBank
RMSD	Root mean square deviation
HIV	Human immunodeficiency virus
WHO	World Health Organization
MDR	Multidrug-resistant
XDR	Extensively drug-resistant
TDR	Totaldrug-resistant
AI	Artificial intelligence
M. tb	*Mycobaterium tuberculosis*
BlaC	Beta-lactamase
MurNAc	N-Acetylmuramic acid
GlcNAc	N-Acetylglucosamine
PG	Peptidoglycan
UDP-GlcNAc	Uridine diphosphate N-Acetylglucosamine
UDP-MurNAc	Uridine diphosphate N-Acetylmuramic acid
Alr	Alanine racemase
Ddl	D-alanine ligase

✉ Umashankar Vetrivel
umashankar.v@icmr.gov.in

[1] Department of Virology and Biotechnology, Bioinformatics Division, Indian Council for Medical Research -National Institute for Research in Tuberculosis (ICMR-NIRT), Chennai, India

[2] Department of Biochemistry and Bioinformatics, Dr. MGR. Janaki College of Arts and Science for Women (Affiliated to University of Madras), Chennai, India

PLP	Pyridoxal 5' phosphate
PMP	Pyridoxamine 5-phosphate
GABA-AT	γ-Aminobutyric acid aminotransferase
DAAT	D-aminoacid aminotransferase
CNS	Central nervous system
DCS	D-Cycloserine
PDB	Protein data bank
MD	Molecular dynamics
OPLS	Optimized potential for liquid simulations
2D	Two-dimensional structure
3D	Three-dimensional structure
UFF	Universal force field
VS	Virtual screening
PyRx	Python prescription
PLIP	Protein-Ligand interaction profiler
LBFGS	Limited-memory Broyden- Fletcher-Goldfarb-Shanno
NPT	Constant number of particle (N), Constant Pressure (P), Constant Temperature (T)
RMSF	Root mean square fluctuation
farPPI	Fast amber rescoring for protein–protein interaction
GAFF2	General amber force field 2
ff14SB	Force field 14, side chain
MMPBSA	Molecular mechanics poisson-boltzmann surface
PB	Poisson-Botzmann
GB	Generalized born
SASA	Solvent-accessible surface area
DCNN	Deep convolutional neural network
SSE	Secondary structural elements
PAINS	Pan assay interference compounds

Introduction

Tuberculosis is caused by the bacterium *Mycobacterium tuberculosis*, which is prevalent globally and has a high mortality rate (Vasava et al. 2017). This infectious disease primarily affects the lungs, leading to pulmonary tuberculosis, and can also affect other parts of the body, causing extra-pulmonary tuberculosis. Tuberculosis is commonly linked to coinfection with HIV and diabetes, with HIV significantly weakening the immune system and increasing the risk of tuberculosis progression (Khan et al. 2019). According to the WHO Global Tuberculosis Report 2024, an estimated 10.84 million individuals developed TB in 2023, yet only 8.16 million were officially diagnosed and reported, leaving approximately 2.7 million cases undetected. Although this represents an improvement from 4.3 million undiagnosed cases in 2020, a substantial proportion of the treatment gap is concentrated in India (16%), Indonesia (11%), Pakistan (7.8%), China (6.5%), and Myanmar (6.5%), collectively accounting for nearly half of the global burden of undiagnosed TB. Current global TB treatment coverage stands at 75%, which remains below the 90% target set for 2027 by WHO, underscoring the urgent need for enhanced diagnostic strategies, strengthened healthcare systems, and increased investment in TB control programs. Addressing these gaps is critical for achieving the End TB Strategy goals, thereby necessitating innovative approaches such as drug repurposing and improved surveillance mechanisms to accelerate case detection and treatment interventions (WHO 2024). Tuberculosis is primarily transmitted through airborne droplets containing *Mycobacterium tuberculosis*, expelled when an infected person coughs or sneezes (Khan et al. 2019). Given the severity and prevalence of tuberculosis, the identification and development of effective antimicrobial drugs are crucial for managing the disease. Existing drug systems encompass multidrug-resistant (MDR), extensively drug-resistant (XDR), total drug-resistant (TDR-TB), and mono-resistant varieties, offering varying degrees of treatment efficacy against the bacterium (Lange et al. 2014; Vasava et al. 2017). Treatment of tuberculosis typically involves the use of a combination of first-line drugs: ethambutol, pyrazinamide, rifampicin, isoniazid, rifabutin, and rifapentine, administered over 6–9 months (Singh et al. 2020; Vasava et al. 2017). In cases where the first-line drugs are not effective, second-line drugs such as fluoroquinolones (e.g., moxifloxacin and levofloxacin) and injectables (e.g., kanamycin, amikacin, and capreomycin) are used (Theron et al. 2014; Vasava et al. 2017). The recent approval of bedaquiline and delamanid for use in MDR/XDR-TB has been a significant breakthrough in tuberculosis drug discovery (Perveen et al. 2022). Clinical trials are currently underway for various tuberculosis drugs in different phases, including TBI-16, GSK-3036656, OPC-167832, SQ109, TB-7371, Q203, Deplazolid, Sutezolid, Contezoild, Macozine, and pretomanid (Muniyandi and Ramachandran 2017; Bahuguna and Rawat 2020). With the continued development of new drugs, there is hope that the fight against tuberculosis can be won. Annually, 1.5 million people face multidrug-resistant tuberculosis, necessitating the development of potent and safe anti-tubercular chemotherapeutics. Drug repurposing, leveraging established medications for new diseases, is a cost-effective strategy that expedites drug discovery, attracting industry and academia. Recent advancements in computational drug repurposing have significantly improved efficiency and accuracy by integrating artificial intelligence (AI), deep learning, and molecular modeling. Machine learning-driven predictive models, combined with molecular docking and molecular

dynamics simulations, facilitate the identification of promising drug candidates with high target binding affinity. AI-assisted virtual screening has further accelerated the evaluation of FDA-approved drugs for various diseases, reducing both the cost and time required for experimental validation (Sahrawat 2024; Samdani and Vetrivel 2018). Numerous drugs have been successfully repurposed to date (Maitra et al. 2016), with example like thalidomide, once used for morning sickness was later suggested for leprosy treatment (Languillon 1971; Maitra et al. 2016). Imatinib, an Abl family tyrosine kinase inhibitors used for certain cancers, has shown promise in killing intracellular Mtb cells (Napier et al. 2011). Potential repurposable drugs for anti-tubercular therapy include antibiotics (linezolid, clofazimine, amikacin, meropenem), non-steroidal anti-inflammatory drugs (diminazene, ebselen), antivirals (isoprinosine), anticancer drugs (bortezomib, elesclomol), cardiovascular drugs (verapamil, simvastatin, pravastatin, terlipressin, desmopressin) and others (metformin, bisbiguanide dihydrochloride, rimonabant, linolenic acid, pranlukast, auranofin, cyclosporin A) (An et al. 2020).

Targeting cell wall synthesis as a potential strategy

The mycobacterial cell envelope is a sophisticated structure comprising peptidoglycan (murein), an arabinogalactan polysaccharide, and mycolic acid. Collectively, these elements contribute to the formation of the intricate mycolyl arabinogalactan-peptidoglycan complex (Van Heijenoort 2001; Abrahams and Besra 2018; Jacobo-Delgado et al. 2023). This complex plays a crucial role in maintaining cellular shape, facilitating the components within the cell, and supporting the growth, persistence, virulence, innate immune response, and overall activity of *Mycobacterium tuberculosis* (*M.tb*) (Jankute et al. 2015; Alderwick et al. 2015; Belete 2022). Acting as an external barrier, it imparts innate resistance to *M.tb* drugs, including ethionamide, isoniazid, ethambutol, and beta-lactam antibiotics targeting the peptidoglycan pathway through beta-lactamase (BlaC) (Jackson et al. 2013; Singh et al. 2017; Hugonnet and Blanchard 2007). Peptidoglycan biosynthesis is a complex process crucial for bacterial protection (Pazos and Peters 2019; Bugg and Walsh 1992) against osmotic lysis, relying on the metabolism of D-Alanine (D-Ala) (Jiang et al. 2021). This linear polymer, forming a net-like structure, is cross-linked by short peptides, contributing to the shape and protection of the bacterial cell (Kuru et al. 2019). Disaccharide polymers, referred to as "glycan strands," linked by ($\beta 1 \rightarrow 4$) glycosidic linkages, contain N-Acetylmuramic acid (MurNAc) and N-acetylglucosamine (GlcNAc) residues, making them a target for antibiotics due to their absence in human cells (Bouhss et al. 2008; Müller et al. 2017; Ogasawara and Dairi 2021).

Initiated in the bacterial cytoplasm, peptidoglycan (PG) biosynthesis involves enzymes GlmS, GlmM, and GlmU synthesizing UDP-GlcNAc. Subsequent steps, catalyzed by MurA and MurB, transform UDP-GlcNAc into UDP-MurNAc. ATP-grasp enzymes (MurC, D, E, and F) sequentially extend the peptide chain to synthesize UDP-MurNAc-pentapeptide (Raymond et al. 2005; Shaku et al. 2020). D-glutamic acid is produced through two routes, and the short peptide in the peptidoglycan monomer is finalized with a D-Ala-D-Ala dipeptide. Essential enzymes, alanine racemase (Alr) and D-alanine ligase (Ddl) play a vital role in D-Ala metabolism (Yang et al. 2018), with their inactivation serving as an effective strategy to prevent bacterial peptidoglycan production and survival (Soda and Tanizawa 1990; Wei et al. 2016) (Fig. 1).

Alanine racemase, a fold type III dependent amino acid racemase enzyme, plays a crucial role in converting L-alanine to D-alanine, a key component in the formation of peptidoglycan within the bacterial cell wall (Strych et al. 2001; Noda et al. 2004; Awasthy et al. 2012). Alr gets inhibited by covalent inhibitors like alanine phosphonate and D-cycloserine (Mehta et al. 2023), and this inhibition was linked to the generation of a stable covalent bond with PLP. All other PLP-containing enzymes have a mechanism that comprises the catalytic steps of proton abstraction and deprotonation (Rubinstein and Major 2010; Azam and Jayaram 2015).

Earlier studies have reported several outline alanine racemase inhibitors for mtb, wherein the docking results highlighted the significant interactions with key amino acid residues (Lys42, Tyr46, Arg140, His172, and Tyr175) that span the binding site of this enzyme (Jayaram and Azam 2022). Numerous studies have evaluated the significance of key binding site residues: Lys42, Tyr46, His172, Arg228, Tyr271, and Met319 in the catalytic steps of enzymes. The potential inhibitors of the alanine racemase are alaphosphin, O-carbamyl-d-serine, chlorovinyl glycine, and d-cycloserine (Azam and Jayaram 2015). For Alr enzymes to function, pyridoxal 5'-phosphate (PLP) is necessary. An internal aldimine bond forms a covalent binding between the cofactor and a lysine side chain on the active site. In the proposed mechanism of inactivation by D-cycloserine (a known inhibitor), it is reported to bind to the Ala site and target the PLP, thereby moving the lysine side chain and creating an external aldimine bond to PLP. In a series of steps, this external aldimine (referred to as "the aldimine") is transformed into a stable isoxazole derivative that resembles pyridoxamine 5-phosphate (PMP), which is considered to act as an irreversible inhibitor. General acids and bases catalyze this reaction. Aldimine, intermediate ketimine, and final isoxazole are structural isomers with the same empirical formula when completely uncharged ($C_{11}H_{14}N_3O_7P$) (de Chiara et al. 2020). Studies on the inactivation of two different PLP-enzymes,

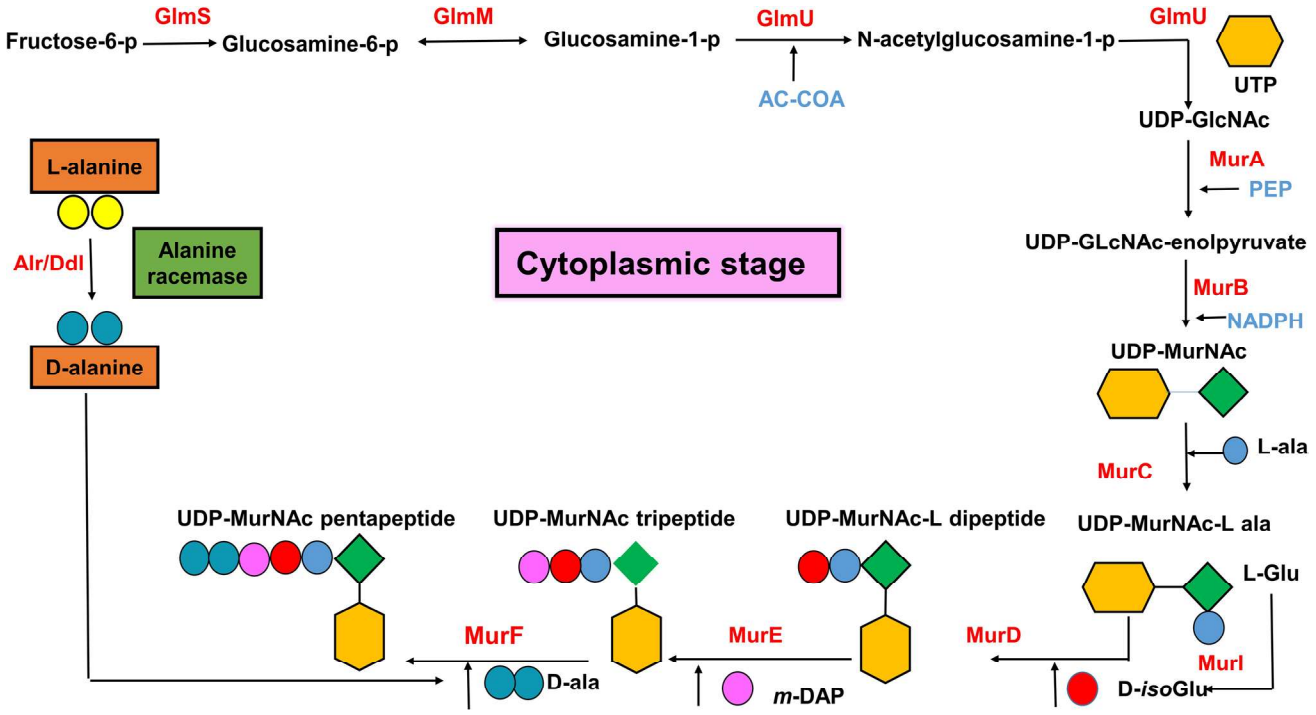

Fig. 1 Synthesis of UDP-NAM pentapeptide in the peptidoglycan biosynthesis in bacterial cell wall

γ-aminobutyric acid aminotransferase (GABA-AT) and d-amino acid aminotransferase (DAAT), by cycloserine led to the original inference of the currently hypothesized inactivation process, known as the "aromatization" mechanism. These studies suggested that the final isoxazole and the other intermediates were connected reversibly for the analogous inactivation of GABA-AT, as well as that the final isoxazole formed during the inactivation of DAAT was irreversible because of the anticipated thermodynamic stability of the aromatic ring. (de Chiara et al. 2020; Peisach et al. 1998; Olson et al. 1998).

As D-cycloserine induces CNS toxicity and also lacks target specificity, its usage is restricted (Azam and Jayaram 2015). It also has adverse effects such as headaches, fatigue, depressive symptoms, vertigo, disorientation, paresthesia, hyperirritability, mental illness, seizure disorders, and jerks are some of the deleterious effects of DCS therapy on the central nervous system. Cycloserine is a cyclic analogue of D-alanine, and it inhibits enzymes by forming covalent conformational changes with the PLP cofactor (Fenn et al. 2003; Court et al. 2021). Other inhibitors, such as alanine phosphonate and propionate, also target PLP and undergo a loss of specificity. Enzyme inhibitors can be designed using three different methods. Placing an inhibitor within the active site is one approach. A second strategy would be blocking entry to the active site by introducing an inhibitor. Designing an inhibitor that would stop dimerization is a third approach. The first approach is the simplest. However, Alr is known to possess a limited active site pocket that makes it challenging to create effective drugs. Adopting the second strategy entails creating compounds that block the entrance. This would solve the issue of access to the active site, but pharmacophore creation would be more challenging (LeMagueres et al. 2003). Designing an inhibitor that restricts entry to the active site is the key objective of this current study. In the current study, we used a virtual screening method to probe the FDA-approved drugs to discover repurposable drugs that could target the alanine racemase enzyme in the peptidoglycan biosynthesis pathway, as it is an essential enzyme in *Mycobacterium tuberculosis*, which is not ubiquitous in humans and serves as a captivating target.

Materials and methods

Structural analysis of alanine racemase

Within PDB, there are two crystal structures available for M.tb alanine racemase: one with co-crystallized ligand (known inhibitor) (D-cycloserine) and PLP bound (as a cofactor) (PDB ID: 6SCZ) and another with PLP in the

native state (PDB ID: 1XFC). The co-crystallized structure (6SCZ) was bound with the cycloserine and PLP, forming an aldimine linkage with the Lys residue. Hence, this structure was only used as a reference for defining the ligand binding residues in the other crystal structure, namely, 1XFC, which had PLP in native unperturbed form and was used for docking of cycloserine, as well as for virtual screening processes. The rationale for choosing 1XFC was based on our earlier attempt in the PLP-dependent enzyme, namely, ornithine Decarboxylase, wherein the usage of the crystal structure with unperturbed PLP yielded significant inferences (Muthukumaran et al. 2021; Sivashanmugam et al. 2019) (Fig. 2).

The alanine racemase structure *Mycobacterium tuberculosis* (mtb (Alr)) used in this investigation (PDB ID: 1XFC) exhibited a resolution of 1.9 Å. Analysis of monomers derived from diverse crystallographic structures revealed a consistent composition of 384 residues per monomer (LeMagueres et al. 2005). The homodimeric enzyme alanine racemase is constituted by a monomer characterized by two distinct domains, mimicking the structural features found in *bacillus* and *pseudomonas* alanine racemases (Shaw et al. 1997; Au et al. 2008; Liu et al. 2012; Yan et al. 2007). The N-terminal region features an eight-stranded α and β-barrel, spanning residues 1–246, while the C-terminal region consists of a β strand extending from residues 247–384 (Fig S1). The two domains of alanine racemase are inclined at an angle of 130° when viewed inside. Amid the two domains, distinct hinge angles can be detected (LeMagueres et al. 2005). The α and β-barrel of one monomer appear against the other monomer. The active site of the alanine racemase is divided into three layers, namely, the inner, intermediate, and outer layers centered around PLP (Fig. 3). Alr *Mtb's* outer layer comprises three residues: Asp357, Lys178, and Ala241.The core layer comprises Tyr271, Tyr364, Tyr290, and Ala176, whereas, the intermediate layer contains Arg316, Ile362, Arg296, and Asp177. This inner layer comprises two tyrosines, Tyr271 and Tyr364, which act as barriers for D-Ala and inhibitors of the PLP binding cavity. It contains two catalytic sites in the C-terminal domain and N-terminal domain. The cofactor called pyridoxal 5'-phosphate is present around and above the edge of the α/β, which is covalently linked through an internal aldimine linkage with Lys 42, which is present at

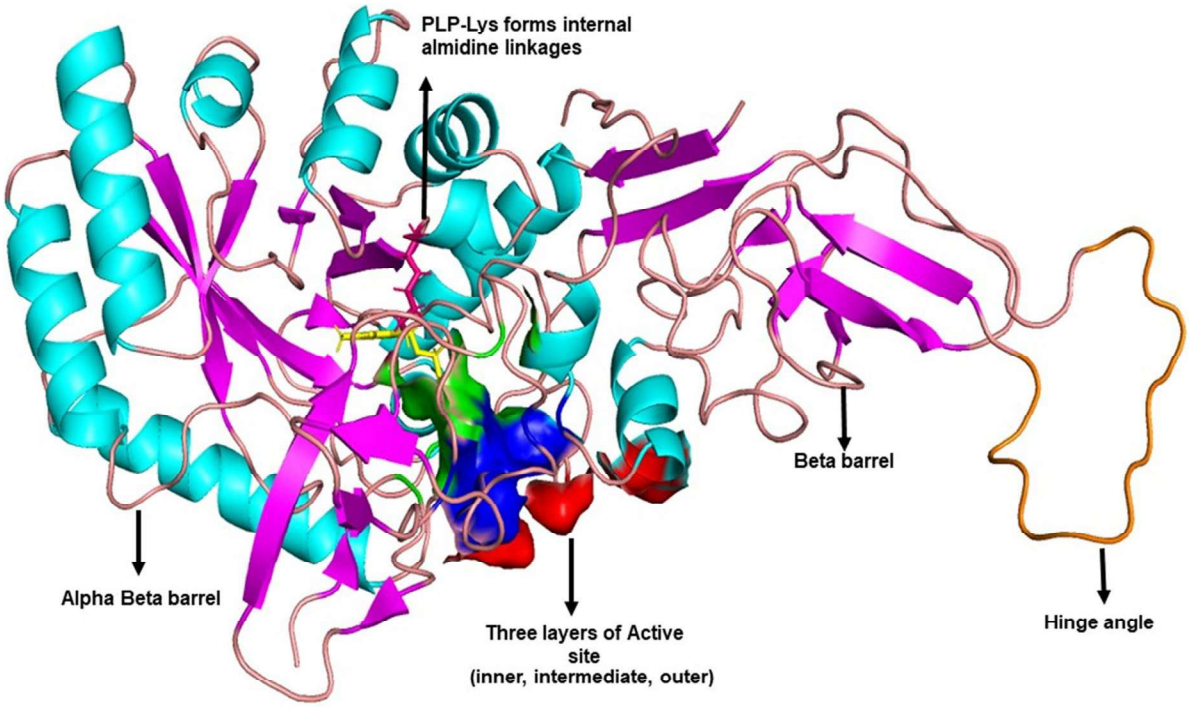

Inner layer	Intermediate	Outer	Cofactor
Try271, Try364, Try290, Ala176	Arg316, Ile362, Arg296, Asp177	Asp357, Lys178, Ala241	PLP381

Fig. 2 Illustrates the secondary structures (α helix-cyan; β sheet-magenta; loops- wheat and hinge-orange), three layers of the active site and cofactor in different colors, and also internal almidine linkages between PLP-Lys in alanine racemase (PDB ID: 1XFC) using PyMOL (PyMOL Molecular Graphics System, Version 2.5.2 Schrodinger, LLC)

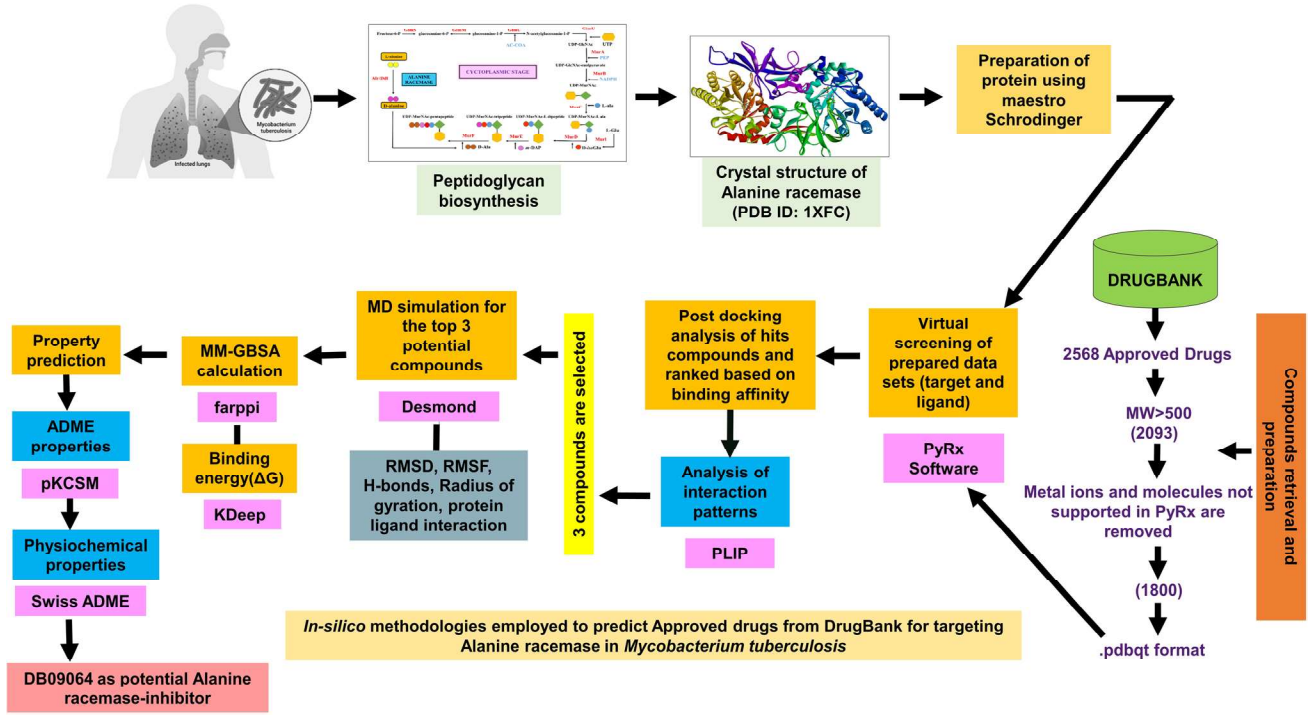

Fig. 3 Schematic representation of workflow in this study

the C-terminal of the β strand of the α and β-barrel (Fig. 2). Corresponding to the PLP cofactor, the substrate binding cavity of *M.tb's* alanine racemase measures approximately 5.5 Å × 5.0 Å × 2.5 Å. The second cavity is opposite to the PLP. There is free space at Trp88, occupied by two water molecules. Because Lys expands its cleft by the monomer's two domains, the PLP moiety is located in the barrel's approximate center, very close to the second domain.

AlrMtb maintains a robust interaction between the N1 atom of PLP and an adjacent arginine, Arg228. A hydrogen bond network is formed among the residues Tyr271, His172, Arg228, and His209. The Schiff base display protonated characteristics due to the strong internal hydrogen bond connection between the imine nitrogen of Lys42 and the O3′ of PLP. Additionally, the phosphate tail of PLP remains stabilized by six hydrogen bonds (LeMagueres et al. 2005). The O3′ atom of PLP forms a new hydrogen bond with the NE1 atom of Trp88 in this structure (Fig. S2). The hydrogen bond interactions involve the single arginine and double tyrosine residues. Several additional residues are involved in directing the PLP structure in this protein. This enzyme's Arg219 forms a hydrogen bond with the pyridine nitrogen and affects electron translocation in PLP alanine intermediates (LeMagueres et al. 2005).

Protein preparation (structure retrieval, refinement, and energy minimization)

The crystal structure of alanine racemase (PDB ID: 1XFC, 1.9 Å), PLP in intact form, was subjected to geometry optimization using the Protein preparation wizard of Schrodinger suite. This module was used to fix bond formation, steric collisions, disulfide bridges, missing loops, and missing residues and to optimize the chi rotation of asparagine, glutamine, and histidine residues. Additionally, histidine protonation states were assigned using Schrodinger's Maestro (Version 12.8) PROPKA at neutral pH, and water molecules within 5 Å of the hetero group were removed using the Protein-preparation module of schrodinger suite. Before being utilized for virtual screening and MD simulations (Kufareva and Abagyan 2012), the optimized protein structure was also energy-minimized using the OPLS 2005 force field (John et al. 2017; Sadhasivam and Vetrivel 2019).

Preparation and filtration of ligand datasets

The FDA(U.S. Food and Drug Administration)-approved ligand datasets were retrieved from DrugBank 5.1.9, which incorporates the experimental drugs, withdrawn, and Nutraceutical

(https://www.drugbank.ca/) (accessed on October 25, 2021) and were proceeded for virtual screening. The dataset comprised 2658 ligands; among these molecules, the ones with molecular weight > 500 kDa were selected, which resulted in 2093 ligands. Out of 2093, the molecules with undesirable atom types like metal ions were expelled by PyRx (version 0.8) software (https://pyrx.sourceforge.io/home) (Dallakyan and Olson (2015) during the ligand filtering process, thereby resulting in 1800 ligands. Further, the 2D structural coordinates of these 1800 ligands in 2D.sdf format were converted to optimal 3D conformations using open babel. The ligands were then subjected to energy minimization using UFF (universal Force Field) with a conjugate gradient method with 200 steps. Finally, all these ligand coordinates were transformed to.pdbqt format for further analysis using Open Babel built-in PyRx (version 0.8) software.

Docking of cycloserine with alanine racemase

The structural coordinates of cycloserine, a known inhibitor of alanine racemase, was retrieved from the ligand depot (http://ligand-depot.rcsb.org/), which was then docked using Autodock Vina embedded in PyRx (version 0.8) to the catalytic site of 1XFC structure. Further, the PLIP (Adasme et al. 2021) server was used to analyze the inter-molecular interactions. The docked complex was superimposed with the co-crystallized structure of alanine racemase (6SCZ with perturbed PLP) to validate the predictive accuracy of the methods implemented. The docked complexes were then assessed for binding free energy (MMGBSA), binding affinity, and complex stability using molecular dynamics simulations (Santos et al. 2019; Barth et al. 1995; Wu et al. 2022).

Virtual screening of alanine racemase against ligands

Autodock Vina, embedded in PyRx (version 0.8) Software wizard, was used to perform the virtual screening (Dallakyan and Olson (2015) FDA-approved drugs against 1XFC (Alr). In this study, AutoDock Vina was used for virtual screening, with the exhaustiveness parameter set to 8 to achieve a thorough exploration of ligand conformations. This parameter determines the depth of sampling, where higher values enhance the likelihood of identifying optimal ligand-binding poses within the protein's active site. An exhaustiveness value of 8 strikes a balance between computational cost and accuracy, ensuring reliable docking outcomes. This approach is widely adopted in structure-based virtual screening to improve the robustness of docking predictions (Samdani and Vetrivel 2018).The catalytic residues chosen for the VS are Tyr271, Tyr364, Tyr290, Ala176, and PLP390 (D-Cycloserine binding site). Grid parameters set: center coordinates of X = 49.83, Y = 22.77, Z = 10.44 with Dimensions (Angstrom) of X = 16.65 Å, Y = 18.85 Å, Z = 18.85 Å. Finally, the protein–ligand interaction patterns of the docked complexes were studied using PLIP online server. (https://plip-tool.biotec.tu-dresden.de/plip-web/plip/index).

Molecular dynamics (MD) simulation of the docked complexes

MD simulation was executed for the docked complexes using the Desmond package with OPLS2005, set as a force field. (Bernardes et al. 2013) (Umashankar et al. 2021). For system building, a simple point charge (SPC/E) explicit water model was used as the solvent, wherein the protein/protein–ligand complexes were centered to a cubic box (10 Å x10Å x 10 Å dimension), and appropriate counter-ions were added to neutralize the system (Nagarajan et al. 2020). Further, the entire system(s) were energy minimized using Steepest Descent and the limited-memory Broyden- Fletcher-Goldfarb-Shanno (LBFGS) algorithms. Moreover, the Ewald particle mesh technique was used during the 200 ns production run to preserve long-range electrostatics (Bulatov et al. 2001; Petersen 1995; Harvey and De Fabritiis 2009). Using an NPT ensemble with a temperature scale of 300 k and pressure of 1.0 bar, the system(s) were equilibrated. Using the Berendsen coupling algorithm (Ryckaert and Ciccotti 1977), the temperature–pressure parameters were coupled (Muralikumar et al. 2017; Umashankar et al. 2021; Berendsen et al. 1984). The well-defined, equilibrated system, including all atoms, were proceeded to a 200 ns production run, with trajectory sampling of 100 ps intervals. The root mean square deviation (RMSD) plots for C-alpha backbone atoms to understand the inter-molecular interactions between proteins and ligands. (Damm and Carlson 2006) were analyzed. The residue-wise root mean square fluctuation (RMSF) plots were analyzed to understand the significant conformational changes in the residues. Additionally, the radius of gyration was measured to assess the structural compactness (Fuglebakk et al. 2012). The 2D interactions of protein–ligand complexes were generated for the complete production run to infer the complexes' long-term durability and interaction sites. (Sadhasivam and Vetrivel 2019; Umashankar et al. 2021). A 200 ns MD simulation was chosen to ensure system equilibration and capture key conformational dynamics of the protein–ligand complexes. Studies indicate that simulations exceeding 100 ns stabilize biomolecular interactions, reducing transient fluctuations, especially in flexible enzymes like alanine racemase (Muthukumaran et al. 2021). This duration allows observation of ligand-induced conformational changes, interaction stability, and binding free energy convergence, ensuring statistically significant structural analyses (RMSD, RMSF, and hydrogen bond occupancy) while maintaining computational efficiency (Sathiyamani et al. 2023).

MM-GBSA calculation of topmost stable complexes

The Molecular Mechanics-Generalized Born Surface Area (MMGBSA) calculation is one of the most extensively used methods for determining the binding free energy of protein–ligand complexes. MM-GBSA implicit solvent modelling and molecular mechanics-based energy calculations are used in this method to precisely calculate the protein–ligand complex binding free energy by contrasting it with the free energies of its unbound constituent parts. Using fast amber rescoring for protein–protein interaction inhibitors (farPPI) on an online web server, the MMGBSA (GB1) calculation was carried out on the most stable complexes (Wang et al. 2019). When compared to other approaches, farPPI's GB1 option was shown to be highly accurate. The server-provided force fields GAFF2 and ff14SB were assigned to the ligand and protein, respectively. The lowest potential energy conformation of the compounds with the best stability was examined (Vivekanandan et al. 2022). Equation: (1)-(4) shows the equations for estimating the MM/PBSA and MM/GBSA binding free energies

$$\begin{aligned} \triangle G_{bind} &= G_{complex} - \left(G_{receptor} + G_{ligand}\right) \\ &= \triangle H - T \triangle S \\ &\approx \triangle E_{MM} + \triangle G_{solv} - T \triangle S \end{aligned} \quad (1)$$

$$\triangle E_{MM} = \triangle E_{bonded} + \triangle E_{ele} + \triangle E_{vdW} \quad (2)$$

$$\triangle G_{solv} = \triangle G_{polar} + \triangle G_{nonpolar} \quad (3)$$

$$\triangle G_{nonpolar} = \gamma \cdot \triangle SASA + \beta \quad (4)$$

The total binding free energy is represented by the ΔG_{bind}. It is the difference in free energy between the bound state (G_{complex}) and Free states ($G_{\text{receptor}} + G_{\text{ligand}}$), and it may alternatively be expressed as the sum of the enthalpy (ΔH) and entropy parts ($-T\Delta S$). Due to their high computational cost and poor accuracy, the entropy changes in this study were ignored while the enthalpy changes were assessed using the MM/PBSA and MM/GBSA techniques. The molecular mechanical energy (ΔE_{MM}) and the solvation-free energy (ΔG_{solv}) may be separated from the enthalpy fraction. As we employed the single MD trajectory procedure in our computations, the ΔE_{MM} term contains the intra-molecular (ΔE_{bondcd}), electrostatic (ΔE_{clc}), and van der Waals (ΔE_{vdW}) energies, where the ΔE_{bonded} is always equal to zero. For polar contributions, the Poisson-Boltzmann (PB) or Generalised Born (GB) model was utilized, whereas, the solvent-accessible surface area (SASA) is thought to be the equivalent for non-polar contributions. MMGBSA improves binding energy estimation by incorporating solvation effects, ligand flexibility, and entropy contributions, unlike traditional docking, which relies on static scoring functions. It enhances predictive accuracy by analyzing dynamic protein–ligand interactions from MD simulations. Additionally, MMGBSA offers a computationally efficient alternative to more complex free energy methods.

Calculation of KDeep for absolute binding affinity (ΔG)

The top-ranking complexes, inferred based on the post-molecular dynamics simulation, were also investigated for absolute binding affinity (ΔG) using KDeep. This computational mode applies 3D convolutional neural networks using a machine learning framework. After receiving the structural input, the DCNN (Deep Convolutional Neural Network) theory-based model—which has been pre-trained using the complete datasets of PDB bind v. 2016 database—calculates the absolute free energy of the protein–ligand complex by evaluating the extent to which the input corresponds to the model. (Jiménez et al. 2018) (https://www.playmolecule.com/Kdeep/) (Vivekanandan et al. 2022). This analysis was performed as an additional entity to validate the binding affinity further.

ADME (absorption, distribution, metabolism, and excretion) predictions

SWISSADME prediction

Poor pharmacokinetic and safety characteristics constitute a significant barrier in drug development, resulting in a high attrition rate. These uncertainties could be reduced with the aid of computational chemistry methods. Thus, the SwissADME web tool (http://www.swissadme.ch/) was also used to calculate the physical and chemical characteristics, lipophilicity, solubility in water, pharmacokinetics, drug-likeness, the BOILED-Egg, iLOGP, and Bioavailability Radar for a better understanding of the ADME properties of the prioritized small molecules. This sort of analysis allows the creation of predictive models of essential ADMET properties for drug development (Daina et al. 2017; Bakchi B et al. 2022).

Results and discussion

Molecular dynamics simulation analysis

MD simulation analysis of the enzyme

The trajectory analysis of the protein RMSD plot revealed that the C-alpha deviations were stable and were within the range of 1.6 Å–3 Å with the average RMSD of 2.3 Å until

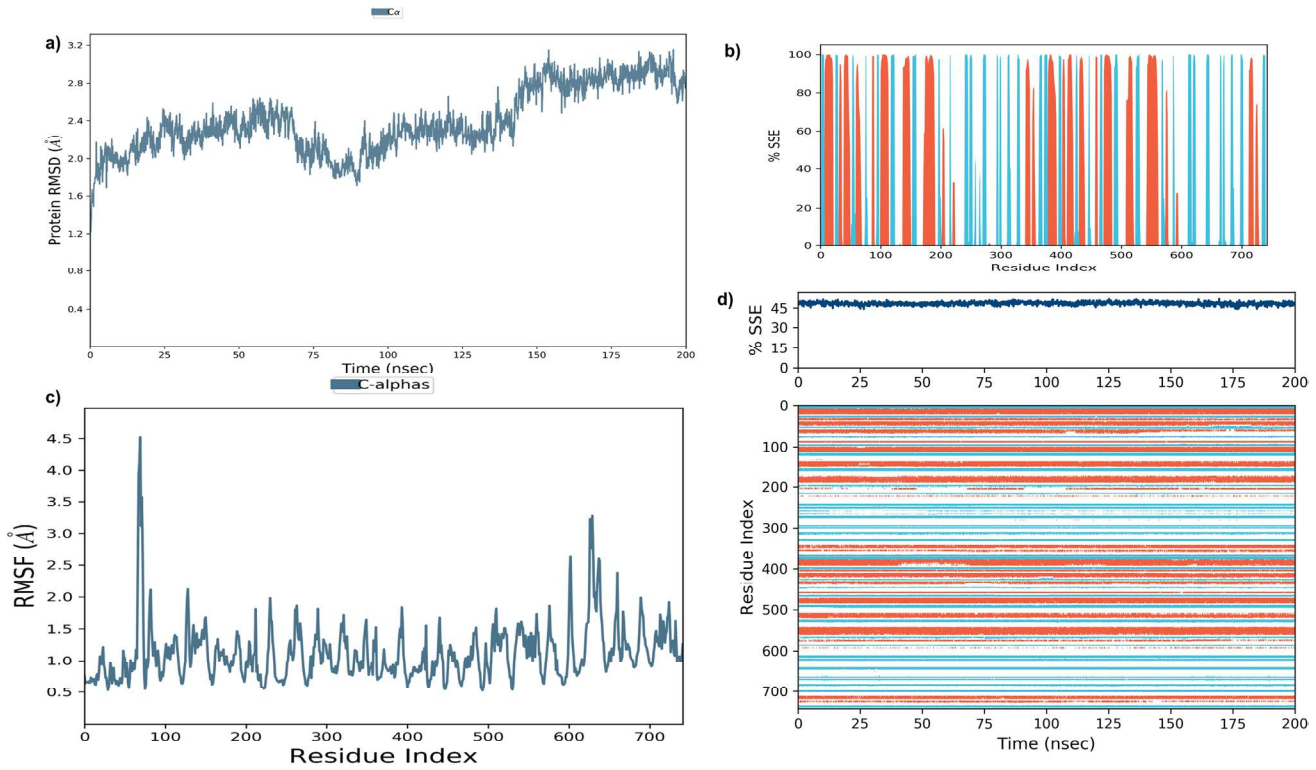

Fig. 4 Depicts the **a** C-alpha RMSD (Root Mean Square Deviation) of *apo* enzyme & **c** RMSF (Root Mean Square Deviation) of *apo* enzyme **b** SSE composition for each trajectory frame over the simulation time **d** % of SSE and monitors each residue throughout the simulation of 200ns

the end of the simulation (Fig. 4a). The RMSF plot also inferred the peaks that represent the most fluctuating residues during the simulation: 75–100 (4.5 Å) and 600–700 (3.2 Å) (Fig. 4c). The dynamics of protein secondary structural elements (SSE) were tracked during the simulation. The following percentages of secondary structure elements conservations were obtained: 26.63% of Helix, 21.66% of strand, and 48.30% of total secondary structure elements. (Fig. 4b) shows the distribution of SSE by residue index across the protein structure. The composition plot also provided an overview of the SSE composition for every trajectory frame sampled. (Fig. 4d).

Post-docking analysis of protein and ligand complex

Alanine racemase and cycloserine (known inhibitor)

The docking of cycloserine, a known inhibitor to alanine racemase (PDB ID:1XFC) showed a docking score of −6.0 kcal/mol. The ligand showed 4 hydrophobic interactions with residues: TYR271 (3.22 Å), TYR290 (3.85 Å), TYR364 (3.50 Å) ILE362 (3.14 Å), hydrogen bonded interactions with LYS42, ARG140, ALA176, ASN212, TYR271, TYR290, TYR364, MET319, ASP320 and also formed salt bridges with HIS172 (3.79 Å).

The co-crystallized (6SCZ-cycloserine) and docked complex (1XFC-cycloserine) exhibited more similar intermolecular interactions (Fig. S3) (Table 1). On superimposition of the complexes, the backbone RMSD value was observed to be 0.264 Å, illustrating the predictive accuracy of the docking protocol adopted.

Post docking analysis of alanine racemase vs. the top-ranking ligands (ciprofibrate, belinostat, flurbiprofen)

The post-docking study revealed that the top 10 complexes (Table S1) had docking scores ranging from −8.0 to −9.0 kcal/mol. Among which the top three ranking drugs were only stringently chosen based on binding affinity and the quantum of intermolecular interactions: flurbiprofen (DB00712), belinostat (DB05015), and ciprofibrate (DB09064) all the three exhibited a similar binding affinity score of −8.5 kcal/mol. The ciprofibrate-alanine racemase complex showed six hydrophobic interactions with chain A-TYR271(3.37 Å, 3.54 Å, 3.85 Å), chain B-TYR 364(3.60 Å) chain B- ILE362 (3.73 Å) and chain A-MET319 (3.61 Å) residues, and also formed hydrogen bonded interactions with TYR290, MET319, ASP320 residues of chain A, and one salt bridge with chain B-LYS42 (3.65 Å). Whereas,

Table 1 Comparison between the residual contacts of cycloserine docked to in 1XFC *vs.* 6SCZ (Co-crystallized with Cycloserine)

Types of interactions	1XFC	6SCZ
Hydrophobic interactions	TYR271A (273A), TYR290A (292A), ILE362B (364B), TYR364B (366B)	TYR90B
Hydrogen bond	LYS42B (44B), ARG140B (142B),ALA176B (178B), ASN212B (214B),TYR271A (273A), TYR290A (292A),MET319A (321A), ASP320A (322A), TYR364B (366B)	LYS44B, TYR48B, TYR90B, ARG142B, SER215B, ARG230B, GLY232B, ILE 233B, TYR273A, TYR292A, MET321A, TYR366B
Salt bridges	HIS172B (174B)	
π- stacking		HIS174B

This study includes two crystal structures: 1XFC (with intact PLP) and 6SCZ (contains PLP in conjugation with D-cycloserine). In the case of 6SCZ, 387 residues have been crystallized while 1XFC had 384 residues been crystallized. Therefore 1XFC had a 3 residue difference when compared to 6SCZ, hence it has a numbering difference as the 3rd residue of the protein is labelled as the 1st residue. To avoid confusion, the actual numbering convention given in the PDB is followed as such. For better clarity, the equivalent residue number in 6SCZ is given in brackets (Table 1)

belinostat-alanine racemase complex showed nine hydrophobic interactions with chain B residues:f ALA176 (3.20 Å, 3.38 Å), ASP177 (3.28 Å), PRO240 (3.53 Å), chain A of TYR271 (3.40 Å), TYR290 (3.66 Å), chain B of ILE362 (3.21 Å, 3.41 Å) and TYR 364 (3.47 Å), six hydrogen bonded interactions with chain B residues namely, LYS42, ALA176 along with chain A residues TYR271, ARG296, MET319, ASP320. A π-stacking with chain B-TYR364 (4.69 Å) was also observed. In case of flurbiprofen, it showed 10 hydrophobic interactions with chain B-ALA176 (3.26 Å), chain A-TYR271 (3.40 Å, 3.52 Å, 3.67 Å) chain A -TYR290 (3.84 Å), chain A -MET319 (3.37 Å), chain B- TYR364 (3.51 Å, 3.62 Å) and chain B -ILE362 (3.40 Å, 3.71 Å). It formed hydrogen bonds with chain A-MET319 and chain A-ASP320. It also featured π-cation interaction with chain A-ARG296 (5.07 Å) and halogenic interactions with chain B-ILE317 (3.77 Å) and 2 salt bridges chain B-LYS42 (3.58 Å) and chain B-ARG140 (5.33 Å) (Table 2) (Fig. S4).

Table 2 Post docking interactions analysis of protein and ligand analysis using PLIP

Drug name/ DrugBank ID/ structures	BA (kcal/mol)	KDeep Δ G (kcal/mol)	Hydrophobic interactions	Hydrogen bonds	Salt bridges	π – stacking	π- cations	Halogens
Flurbiprofen (DB00712) 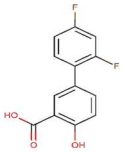	-8.5	-7.19	ALA176B (178B), TYR271A (273A), TYR290A (292A), MET319A (321A), ILE362B (364B), TYR364B (366B)	MET319A (321A), ASP320A (322B)	LYS42B (44B), ARG140B (142B)		ARG296 A (298A)	ILE317A (319A)
Ciprofibrate (DB09064) 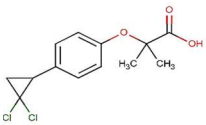	-8.5	-7.53	TYR271A (273A), TYR290A (292A), MET319A (321A), ILE362B (364B), TYR364B (366B)	TYR290A (292A), MET319A (321A), ASP320A (322A)	LYS42B (44B)			
Belinostat (DB05015) 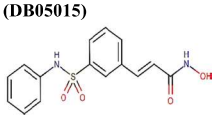	-8.5	-8.64	ALA176B (178B), ASP177B (179B), PRO240B (242B), TYR271A (273A), ILE362B (364B), TYR364B (366B)	LYS42B (44B), ALA176B (178B), TYR271A (273A), ARG296A (298A), MET319A (321A), ASP320A (322A)		TYR364B (366B)		

As this study includes two crystal structures: 1XFC (with intact Pyridoxal 5′- Phosphate (PLP)) and 6SCZ (contains PLP in conjugation with D-cycloserine). In the case of 6SCZ, 387 residues have been crystallized while 1XFC had 384 residues been crystallized. Therefore 1XFC had a 3 residue difference when compared to 6SCZ, hence it has a numbering difference as the 3rd residue of the protein is labelled as the 1st residue. To avoid confusion, the actual numbering convention given in the PDB is followed as such. For better clarity, the equivalent residue number in 6SCZ is given in brackets (Table 2)

ADMETox prediction for the top three compounds

SWISS ADME prediction

The physicochemical properties like molecular formula, molecular refractivity, and consensus log for the top three ranking compounds were calculated. All these three compounds demonstrated optimum ADME qualities with no substantial violations and were also found to adhere to the Lipinski, Ghose, Verber, Egan, and Muegge criteria, whereas cycloserine adheres to only three (Lipinski, Verber, Egan) regulations. Ciprofibrate, belinostat, flurbiprofen, and cycloserine also featured bioavailability scores of 0.85, 0.55, 0.85, and 0.55, respectively. Among these, ciprofibrate and belinostat were featured as lead-like compounds. All these compounds do not violate PAINS. Three compounds have promising synthetic accessibility values of 2.41, 2.94, 2.45, and 2.73 (Table S2).

MD simulation analysis of *Holo* forms

Alanine racemase-cycloserine complex

The system tends to achieve convergence at 30 ns with an RMSD of ~ 3.0 Å, which was maintained throughout the simulation. From 0–30 ns, the C-α RMSD ranged between 1.5 Å and 2.2 Å. The overall average RMSD was observed to be ~ 2.3 Å (Fig. 5a). The residue-wise RMSF plot analysis revealed a minimal variation of approximately 3.0 Å and a maximum fluctuation of 4.2 Å, indicating the mobility of the compound to be constrained within the complex. A favorable association between the ligand and protein (considering both chains) was seen in the residue stretches: 400–600, 700–720, and 250–310, as observed in the RMSF plot (Fig. S5a). (Fig. S6a) indicates that the ligand atoms 9 and 21 fluctuate to a maximum of ~ 2.0 Å. Various interactions such as hydrophobic, water bridges, ionic, and hydrogen bonds were observed in residues TYR 271A, HIS 273A, MET319A, LYS42B, HIS172B, MET173B, VAL174B, ASP177B, and ASN 212B, while ASP 320A exhibited hydrogen bonded interactions and water bridges throughout the simulations, within the range of 0–70%. The protein–ligand complex displayed 6–12 contacts up to 50 ns, 1–5 contacts from 50–100 ns, 5–12 contacts from 100–125 ns, and 1–8 contacts from 125–200 ns (Fig. 6a). The structural compactness was constant during the simulation. In the case of the Rg (radius of gyration) plot, 3.30 Å to 3.45 Å of variation was observed (Fig. S7a). Ligand torsion plot analysis revealed ten rotatable bonds between the atomic pairs: 4–21, 5–10, 10–2, 2–11, 13–16, 6–14, 14–17, 17–22, 19–22, and 20–22 (Fig. S8a). The conformational deviations of each rotatable bond during the simulation (0–200 ns) are illustrated by this ligand torsions plot(Fig. S8).

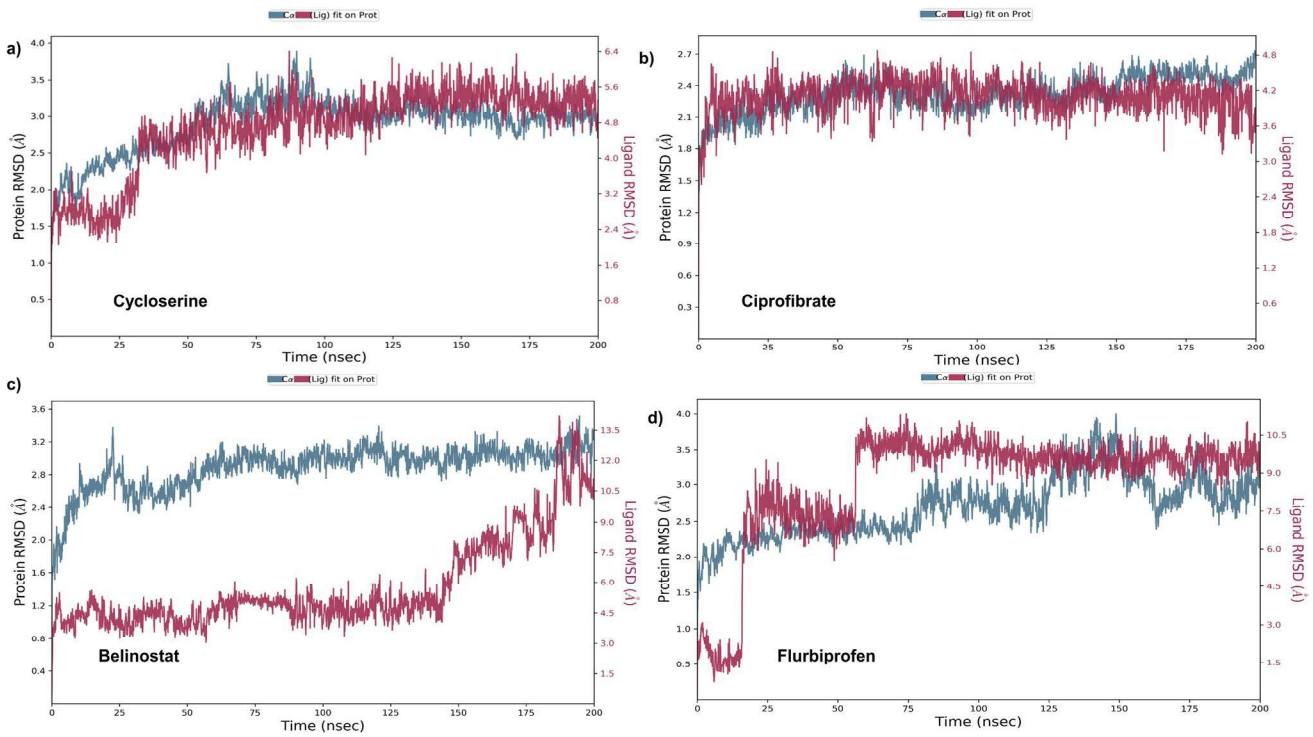

Fig. 5 The C-α root mean square deviation of holoenzyme-ligand complexes for 200 ns

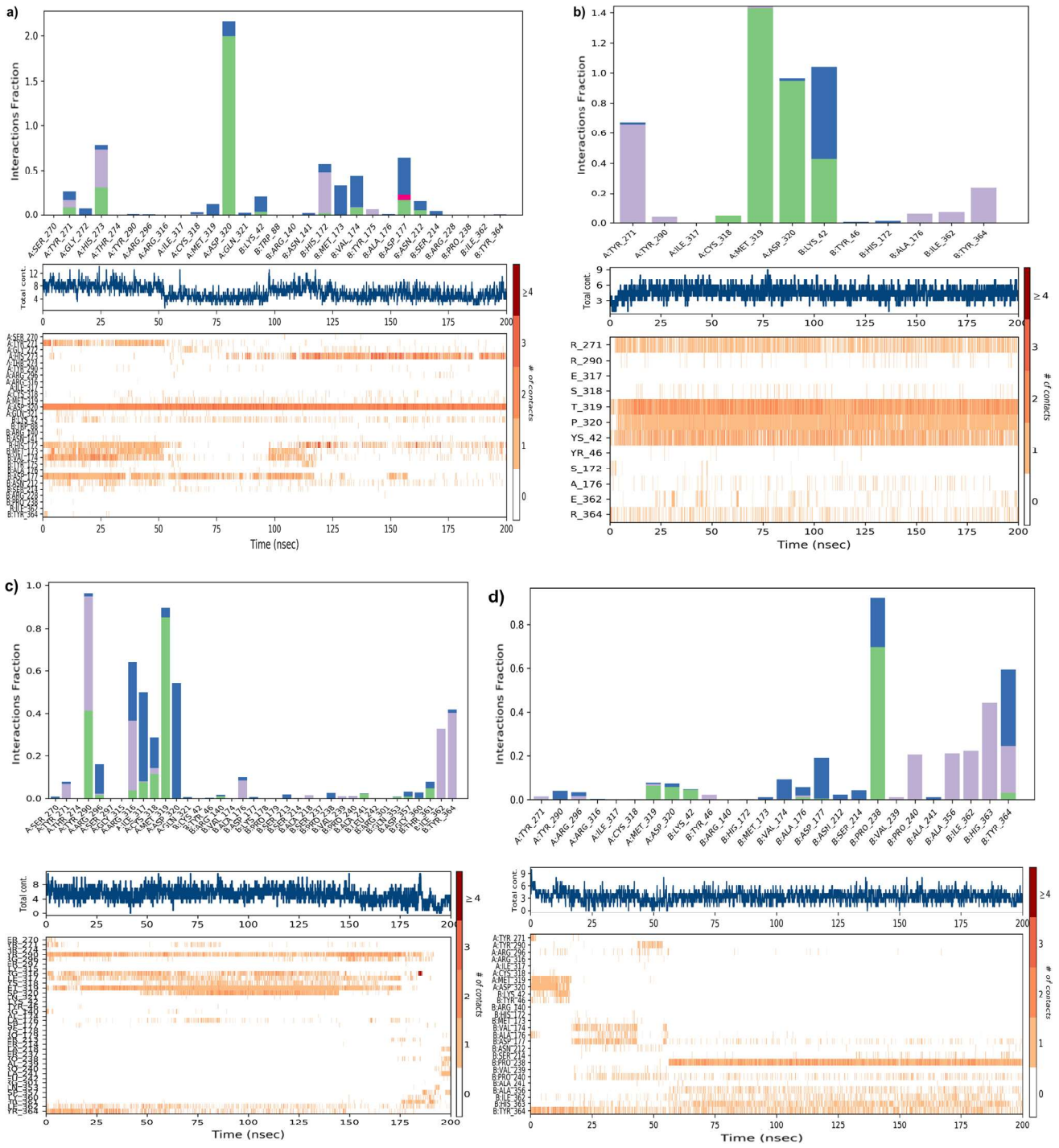

Fig. 6 Protein–ligand contacts of **a** Alr-known inhibitor (cycloserine) and **b** Alr-ciprofibrate (DB09064) **c** Alr-belinostat (DB05015) and **d** Alr-flurbiprofen (DB00712)

Alanine racemase-ciprofibrate complex

During the simulation process, the protein and ligand remained in close contact within the binding cavity, with an RMSD range of 1.5 Å to 2.5 Å and an average of 2.1 Å. The complex was shown to remain stable throughout the simulation, with system convergence occurring at 50 ns in the ligand-bound state (Fig. 5b). The RMSF plot indicated stablization at residue stretches: 260–310, 400–540, and 720 (Fig. S5b). Moreover, the atoms 12, 17, and 18 of the ligands exhibited fluctuations ranging from 1.1 Å to 2 Å (Fig. S6b).

On analyzing the protein–ligand contacts across the trajectory, it revealed that ligands form specific interactions, such as hydrophobic interactions and water bridges with TYR 271A, hydrophobic interactions and a strong hydrogen bond with MET 319A, water bridges and strong hydrogen bonds in ASP 320A, hydrogen bond as well as water bridges with LYS 32B, hydrophobic interactions with TYR 364B. The ligand showed varying numbers of contacts at different time points, with 0–3 contacts until 10 ns and 3–7 stable contacts till 200 ns (Fig. 6b). The Rg analysis also indicated structural compactness, with Rg values ranging from 3.9 Å to 4.1 Å throughout the production run. This ligand also exhibited four internal hydrogen bonds ranging from 75–100 ns to 150–200 ns (Fig. S7b). The ligand possessed six rotatable bonds at atomic pairs: 11–1, 4–14, 14–7, 7–10, 16–10, and 10–5 (Fig. S8b).

Alanine racemase-belinostat complex

The protein exhibited an average C-α RMSD of 1.8 Å, with a range of 0.8 Å to 2.8 Å. deviation. Convergence was observed on the RMSD plot at 180 ns, with a difference of ~ 3.2 Å in the ligand-bound state (Fig. 5c). The RMSF plot also indicated indicated stablization at residue stretches: 250–310, 400–410, 500–600, and 600–720 (Fig. S5c). Fluctuations were also observed in the ligand atoms 2, 11, 12, 16, 17, and 21 (Fig. S6c).

According to the protein–ligand contact analysis, TYR 290A exhibited hydrogen-bonded interactions, hydrophobic interactions, and water bridges 98% of the time. MET319A showed hydrogen bond and water bridge interactions 90% of the time. ARG316A and CYS318A displayed a range of interactions including hydrogen bonds, hydrophobic interactions, and water bridges, accounting for 30% to 65% of the time. ASP320A showed 55% interactions with water bridges. ILE362B exhibited hydrophobic interactions for 35% of the time. TYR364B showed interactions between hydrophobic and water bridges 40% of the time. The protein–ligand complex also maintained 3 to 9 contacts from 0 to 150 ns, and 3 to 5 contacts from 150 to 200 ns (Fig. 6c). Rg values ranged from 3.3 Å to 3.7 Å during the simulation, indicating that the complex had retained structural compactness. The ligand also showed one internal hydrogen bond between 175–200 ns (Fig. S7c). The ligand contained 7 rotatable bonds, specifically between atomic pairs: 21- 2, 2 –17, 17- 16, 5–5, 3–22, 22–1, and 1–9 (Fig. S8c). The percentages of secondary structure elements maintained during the complex simulation are as follows: helices accounting for 24.41%, strands for 21.48%, and the total secondary structure elements accounting for 45.89% (Fig. S9c). Protein–ligand complex interactions are also illustrated in a two-dimensional form as seen in (Fig. 7c).

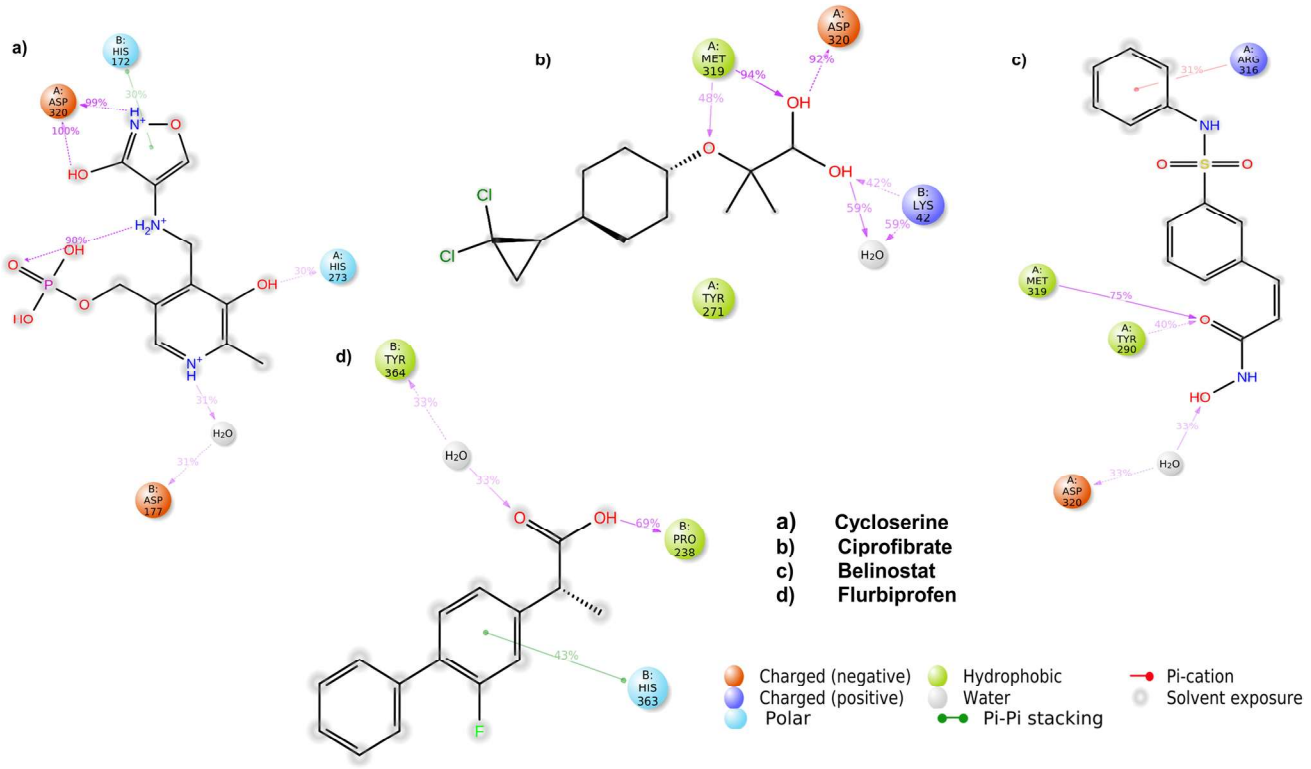

Fig. 7 2D representation of protein–ligand contacts for the entire 200 ns

Alanine racemase-flurbiprofen complex

The C-apha RMSD values of the alanine racemase-flurbiprofen complex ranged from 0.5 Å to 1.0 Å during 0–20 ns, and it ranged from 2.3 Å to 3.3 Å during 21–55 ns. At 60 ns, the ligand exhibited increased deviation with an RMSD of ~ 3.2 Å to 3.8 Å, and the convergence was also observed at 50 ns. The protein C-α showed an average RMSD of 2.0 Å (Fig. 5d). The residue stretches: 250–310, 400–410, 500–600, and 600–720 showed favorable fluctuation, as per the RMSF plot (Fig. S5d). Fluctuations were observed in ligand atoms stretches 12–14 and 16–18, ranging from 3.5 Å to 4.0 Å (Fig. S6d). The ligand also showed intermolecular interactions such as water bridges, hydrogen bonds, and hydrophobic interactions with various residues including TYR 271A, TYR 290A, ARG 296A, MET 319A, ASP 320A, LYS42B, TYR 46B, VAL 174B, ALA 176B, ASP 177B, ASN 212B, and SER 214B. PRO 238B also exhibited hydrogen bonds and water bridges for approximately 90% of the time, while PRO 240B, ALA 356B, ILE 362B, and HIS 363B showed varying degrees of hydrophobic interactions (20–55%). TYR 364B showed hydrogen bonds, and hydrophobic and water bridge interactions for approximately 60% of the time. The protein–ligand complex showed 3–7 intermolecular contacts throughout the simulation (Fig. 6d). The Rg values ranged from 3.50 Å to 3.60 Å, indicating that the complex has maintained structural compactness during the simulation (Fig. S7d). The ligand possessed four rotatable bonds between 1 and 7, 7 and 9, 9 and 17, and 10 and 2 atoms (Fig. S8d). Protein–ligand complexes interactions were visualized in two dimensions as shown in (Fig. 7d) using Schrodinger's maestro (Version 12.8).

Ciprofibrate stands out as the most promising compound due to its superior structural stability and favorable interaction patterns with alanine racemase. This suggests its potential as a lead candidate for anti-TB drug development.

Across all complexes, residue stretches (considering both chains) such as 250–310, 400–600, and 600–720 were identified as critical regions for maintaining stability and ligand interaction. The intermolecular interactions, including hydrophobic interactions, hydrogen bonds, water bridges, and salt bridges, were pivotal in stabilizing the protein–ligand complexes. The identified interactions and structural stability reinforce the potential of ciprofibrate, belinostat, and flurbiprofen as viable alanine racemase inhibitors. Among these, ciprofibrate demonstrated superior stability and interaction patterns, highlighting its potential as a hit for further anti-TB drug development.

Discussion

Tuberculosis (TB) continues to pose a significant global health challenge, particularly in low- and middle-income countries, where it remains a leading cause of mortality and morbidity. The emergence of drug-resistant TB has intensified this crisis, underscoring the urgent need for innovative therapeutic strategies. This study employed a computational drug repurposing strategy to identify potential inhibitors targeting alanine racemase, a critical enzyme in the peptidoglycan biosynthesis pathway which is absent in humans. Virtual Screening FDA-approved drugs from DrugBank 5.1.9, followed by comparative molecular docking studies using cycloserine, a known alanine racemase inhibitor has led to the identification of three potential candidates: ciprofibrate (DB09064: Targets PPAR-alpha and is used to treat hyperlipidemia), belinostat (DB05015: Targets histone deacetylases (HDACs) and is approved for peripheral T-cell lymphoma), Flurbiprofen (DB00712: Targets COX-1 and COX-2 and is used for pain, inflammation, and arthritis) (www.drugbank.com). All three candidates demonstrated strong binding affinities and favorable interaction profiles within the active site of alanine racemase. Molecular mechanics generalized Born surface area (MMGBSA) and free energy change (ΔG) analyses confirmed the stability and potential efficacy of these compounds. Among these candidates, ciprofibrate (DB09064) stood out as the most potential hit. Its strong binding stability, robust interactions within the active site of alanine racemase, and similarity to cycloserine in interaction patterns and structural stability (RMSD) during MD simulations highlights its potential efficacy. These findings provide a strong rationale for exploring ciprofibrate as a potential moiety for consideration into preclinical and subsequent clinical studies as a novel treatment for drug-resistant TB. However, recent studies raise concerns about the use of fibrates in tuberculosis (TB) treatment (Liu et al. 2020). Notably, fenofibrate, a widely used lipid-lowering drug, has been found to promote *Mycobacterium tuberculosis* (Mtb) survival in macrophages as per in vitro studies. This effect is linked to its ability to alter lipid metabolism, increasing intracellular lipid accumulation an environment that favors Mtb persistence and growth. However, it should be noted that In vitro bacterial survival and concentration measurements do not fully replicate the complex growth dynamics of Mtb within a host environment (Liu et al. 2020). While Ciprofibrate shares structural similarities with other fibrates, there is currently no experimental data confirming whether it promotes or inhibits Mtb survival in macrophages. This remains an open question requiring direct investigation, as Ciprofibrate exhibits differential pharmacokinetics and molecular interactions compared to other fibrates.

Despite these concerns, ciprofibrate presents a unique opportunity for repurposing in TB therapy. Our docking and molecular dynamics simulations suggest that ciprofibrate binds strongly to Mtb's alanine racemase, an essential enzyme for bacterial cell wall synthesis. Unlike fenofibrate's indirect effects on host metabolism, ciprofibrate may also exert a more direct antibacterial action by targeting a key

metabolic enzyme. However, given the metabolic effects seen with other fibrates, it is crucial to investigate whether ciprofibrate similarly influences host lipid metabolism and Mtb survival. Further in vitro and in vivo studies will be essential to determine its potential as a viable TB therapeutic. If validated and found suitable, this repurposed drug could offer a cost-effective and readily available therapeutic option, particularly in high-burden regions.

This study underscores the value of computational drug repurposing in addressing the critical need for new TB therapeutics. Beyond identifying potential inhibitors, it highlights the importance of detailed structural and thermodynamic analyses to validate drug-target interactions. These insights can streamline the drug discovery process, reducing costs and development timelines. Future research should focus on preclinical and in vivo evaluations of ciprofibrate to assess its pharmacokinetics, efficacy, and safety for TB treatment. Additionally, exploring combinatorial therapies involving ciprofibrate and existing anti-TB drugs may enhance treatment outcomes, particularly against multidrug-resistant TB strains. The continued advancement of computational approaches holds great promise for uncovering new therapeutic avenues, ultimately contributing to more effective TB management strategies.

Conclusion

In conclusion, this study highlights the urgent need for new treatment strategies to combat tuberculosis (TB), especially as drug-resistant *Mycobacterium tuberculosis* (Mtb) strains continue to rise. Using a computational drug repurposing approach, we predicted potential inhibitors of alanine racemase, a key enzyme in bacterial cell wall biosynthesis. Screening FDA-approved drugs from DrugBank 5.1.9, followed by molecular docking and comparative analyses with cycloserine, a known Alr inhibitor, revealed three potential candidates: ciprofibrate, belinostat, and flurbiprofen which showed appreciable binding affinities, stable interactions, and favorable drug-like properties. Among these, ciprofibrate, a fibrate used to lower cholesterol, exhibited strong binding stability and most favorable interactions within the Alr active site. Unlike fenofibrate, a prodrug requiring hepatic activation, ciprofibrate is an active drug with a lower molecular weight, which may influence differential pharmacokinetics and molecular interactions. However, its potential effects on Mtb remain untested, and the broader implications of fibrate use in TB therapy are still unclear. Fenofibrate, have been shown to modulate lipid metabolism in macrophages, potentially enhance Mtb persistence in vitro, however, it should be noted that In vitro bacterial survival and concentration measurements do not fully mimic Mtb growth dynamics in a host environment. While ciprofibrate shows computational promise, rigorous experimental validation is essential to confirm its therapeutic potential. Given these uncertainties, lead optimization is essential to refine this compound towards improving its binding affinity, specificity, and pharmacokinetics while reducing off-target effects. Fragment-based drug design (FBDD), free energy perturbation (FEP), and molecular dynamics simulations could help optimize its efficacy. While this study lays the groundwork for repurposing ciprofibrate and related compounds, extensive experimental validation including enzyme inhibition assays, bacterial growth studies, and host–pathogen interaction models is crucial to assess their real-world potential. Ultimately, this research highlights the power of computational drug repurposing in accelerating TB drug discovery and underscores the importance of a multidisciplinary approach to validate and optimize promising candidates.

Supplementary Information The online version contains supplementary material available at https://doi.org/10.1007/s11756-025-01916-5.

Author contributions Keerthika LakshmanaPerumal: Writing – original draft, Methodology, Investigation, Formal analysis, Data curation; Umashankar Vetrivel: Conceptualization, Writing and reviewing—draft, Methodology, tools, Formal analysis.

Funding N/A.

Data availability All the raw data used in this manuscript are download from publicly available databases.

Declarations

Ethical approval This study is purely computational and hence does not involve Ethical concerns.

Informed consent N/A.

Conflict of interest Authors declare no conflict of interest.

References

Abrahams KA, Besra GS (2018) Mycobacterial cell wall biosynthesis: a multifaceted antibiotic target. Parasitology 145:116–133. https://doi.org/10.1017/S0031182016002377

Adasme MF, Linnemann KL, Bolz SN, Kaiser F, Salentin S, Haupt VJ, Schroeder MPLIP (2021) Expanding the scope of the protein–ligand interaction profiler to DNA and RNA. Nucleic Acids Res 49:W530–W534. https://doi.org/10.1093/nar/gkab294

Alderwick LJ, Harrison J, Lloyd GS, Birch HL (2015) The mycobacterial cell wall-peptidoglycan and arabinogalactan. Cold Spring Harb Perspect Med 5(8):a021113. https://doi.org/10.1101/cshperspect.a021113

An Q, Li C, Chen Y, Deng Y, Yang T, Luo Y (2020) Repurposed drug candidates for antituberculosis therapy. Eur J Med Chem 192:112175. https://doi.org/10.1016/j.ejmech.2020.112175

Au K, Ren J, Walter TS, Harlos K, Nettleship JE, Owens RJ, Stuart DI, Esnouf RM (2008) Structures of an alanine racemase from *Bacillus anthracis* (BA0252) in the presence and absence of (R)-1-aminoethylphosphonic acid (L-Ala-P). Acta crystallogr. Sec F,

Struct Biol and crystallization communications 64(Pt 5):327–333. https://doi.org/10.1107/S1744309108007252

Awasthy D, Bharath S, Subbulakshmi V, Sharma U (2012) Alanine racemase mutants of mycobacterium tuberculosis require D-alanine for growth and are defective for survival in macrophages and mice. Microbiology (Reading, England) 158(Pt 2):319–327. https://doi.org/10.1099/mic.0.054064-0

Azam MA, Jayaram U (2015) Inhibitors of alanine racemase enzyme: a review. J Enzyme Inhib Med Chem 31(4):517–526. https://doi.org/10.3109/14756366.2015.1050010

Bahuguna A, Rawat DS (2020) An overview of new antitubercular drugs, drug candidates, and their targets. Med Res Rev 40(1):263–292. https://doi.org/10.1002/med.21602

Bakchi B, Krishna AD, Sreecharan E, Ganesh VBJ, Niharika M, Maharshi S, Puttagunta SB, Sigalapalli DK, Bhandare RR, Shaik AB (2022) An overview on applications of SwissADME web tool in the design and development of anticancer, antitubercular and antimicrobial agents: a medicinal chemist's perspective. J Mol Struct 1259:132712. https://doi.org/10.1016/j.molstruc.2022.132712

Barth E, Kuczera K, Leimkuhler, BJ, Skeel, RD (1995) Algorithms for constrained molecular dynamics. J Comput Chem 16. https://doi.org/10.1002/jcc.540161003

Belete TM (2022) Recent progress in the development of novel mycobacterium cell wall inhibitor to combat drug-resistant tuberculosis. Microbiology Insights 15:11786361221099878. https://doi.org/10.1177/11786361221099878

Berendsen HJC, Postma JPM, van Gunsteren WF, Dinola A, Haak JR (1984) Molecular dynamics with coupling to an external bath. J Chem Phys 81:3684–3690. https://doi.org/10.1063/1.448118

Bernardes CE, Canongia Lopes JN, Minas da Piedade ME (2013) All-atom force field for molecular dynamics simulations on organotransition metal solids and liquids. application to M(CO)(n) (M = Cr, Fe, Ni, Mo, Ru, or W) compounds. J Phys Chem A 117(43):11107–11113. https://doi.org/10.1021/jp407739h

Bouhss A, Trunkfield AE, Bugg TDH, Mengin-Lecreulx D (2008) The biosynthesis of peptidoglycan lipid-linked intermediates. FEMS Microbiol Rev 32:208–233. https://doi.org/10.1111/j.1574-6976.2007.00089.x

Bugg TD, Walsh CT (1992) Intracellular steps of bacterial cell wall peptidoglycan biosynthesis: enzymology, antibiotics, and antibiotic resistance. Nat Prod Rep 9(3):199–215. https://doi.org/10.1039/np9920900199

Bulatov VV, Justo JF, Cai W, Yip S, Argon AS, Lenosky T, Koning MD, Rubia TD (2001) Parameter-free modelling of dislocation motion: the case of silicon. Philos Mag A 81(5):1257–1281. https://doi.org/10.1080/01418610108214440

Court R, Centner CM, Chirehwa M, Wiesner L, Denti P, de Vries N, Harding J, Gumbo T, Maartens G, McIlleron HN (2021) Neuropsychiatric toxicity and cycloserine concentrations during treatment for multidrug-resistant tuberculosis. Int J Infect Dis 105:688–694. https://doi.org/10.1016/j.ijid.2021.03.001

Daina A, Michielin O, Zoete V (2017) SwissADME: a free web tool to evaluate pharmacokinetics, drug-likeness and medicinal chemistry friendliness of small molecules. Sci Rep 7:42717. https://doi.org/10.1038/srep42717

Dallakyan S, Olson AJ (2015) Small-molecule library screening by docking with pyrx. Methods Mol Biol (Clifton, N.J.) 1263:243–250. https://doi.org/10.1007/978-1-4939-2269-7_19

Damm KL, Carlson HA (2006) Gaussian-weighted RMSD superposition of proteins: a structural comparison for flexible proteins and predicted protein structures. Biophys J 90(12):4558–4573. https://doi.org/10.1529/biophysj.105.066654

de Chiara C, Homšak M, Prosser GA, Douglas HL, Garza-Garcia A, Kelly G, Purkiss AG, Tate EW, de Carvalho LPS (2020) D-Cycloserine destruction by alanine racemase and the limit of irreversible inhibition. Nat Chem Biol 16(6):686–694. https://doi.org/10.1038/s41589-020-0498-9

Fenn TD, Stamper GF, Morollo AA, Ringe D (2003) A side reaction of alanine racemase: transamination of cycloserine. Biochemistry 42(19):5775–5783. https://doi.org/10.1021/bi027022d

Fuglebakk E, Echave J, Reuter N (2012) Measuring and comparing structural fluctuation patterns in large protein datasets. Bioinformatics (Oxford, England) 28(19):2431–2440. https://doi.org/10.1093/bioinformatics/bts445

Harvey MJ, De Fabritiis G (2009) An Implementation of the smooth particle mesh ewald method on gpu hardware. J Chem Theory Comput 5(9):2371–2377. https://doi.org/10.1021/ct900275y

Hugonnet JE, Blanchard JS (2007) Irreversible inhibition of the *Mycobacterium tuberculosis* beta-lactamase by clavulanate. Biochemistry 46(43):11998–12004. https://doi.org/10.1021/bi701506h

Jackson M, McNeil MR, Brennan PJ (2013) Progress in targeting cell envelope biogenesis in *Mycobacterium tuberculosis*. Future Microbiol 8(7):855–875. https://doi.org/10.2217/fmb.13.52

Jacobo-Delgado YM, Rodríguez-Carlos A, Serrano CJ, Rivas-Santiago B (2023) *Mycobacterium tuberculosis* cell-wall and antimicrobial peptides: a mission impossible? Front Immunol 14:1194923. https://doi.org/10.3389/fimmu.2023.1194923

Jankute M, Cox JA, Harrison J, Besra GS (2015) Assembly of the mycobacterial cell wall. Annu Rev Microbiol 69:405–423. https://doi.org/10.1146/annurev-micro-091014-104121

Jayaram U, Azam MA (2022) Computational molecular modeling studies of some *Mycobacterium tuberculosis* alanine racemase inhibitors. Acta Chim Slov 69(2):393–404. https://doi.org/10.17344/acsi.2021.7267

Jiang Q, He X, Shui Y, Lyu X, Wang L, Xu L, Chen Z, Zou L, Zhou X, Cheng L, Li M (2021) d-Alanine metabolic pathway, a potential target for antibacterial drug designing in *Enterococcus faecalis*. Microb Pathog 158:105078. https://doi.org/10.1016/j.micpath.2021.105078

Jiménez J, Škalič M, Martínez-Rosell G, De Fabritiis G (2018) KDEEP: protein-ligand absolute binding affinity prediction via 3D-convolutional neural networks. J Chem Inf Model 58(2):287–296. https://doi.org/10.1021/acs.jcim.7b00650

John A, Sivashanmugam M, Umashankar V, Natarajan SK (2017) Virtual screening, molecular dynamics, and binding free energy calculations on human carbonic anhydrase IX catalytic domain for deciphering potential leads. J Biomol Struct Dyn 35(10):2155–2168. https://doi.org/10.1080/07391102.2016.1207565

Khan MK, Islam MN, Ferdous J, Alam MM (2019) An overview on epidemiology of tuberculosis. Mymensingh Medical Journal : MMJ 28(1):259–266

Kufareva I, Abagyan R (2012) Methods of protein structure comparison. Methods Mol Biol (Clifton, N.J.) 857:231–257. https://doi.org/10.1007/978-1-61779-588-6_10

Kuru E, Radkov A, Meng X, Egan A, Alvarez L, Dowson A, Booher G, Breukink E, Roper DI, Cava F, Vollmer W, Brun Y, VanNieuwenhze MS (2019) Mechanisms of incorporation for D-Amino acid probes that target peptidoglycan biosynthesis. ACS Chem Biol 14(12):2745–2756. https://doi.org/10.1021/acschembio.9b00664

Lange C, Abubakar I, Alffenaar JW, Bothamley G, Caminero JA, Carvalho AC, Chang KC, Codecasa L, Correia A, Crudu V, Davies P, Dedicoat M, Drobniewski F, Duarte R, Ehlers C, Erkens C, Goletti D, Günther G, Ibraim E, Kampmann B, Kuksa L, de Lange W, van Leth F, van Lunzen J, Matteelli A, Menzies D, Monedero I, Richter E, Rüsch-Gerdes S, Sandgren A, Scardigli A, Skrahina A, Tortoli E, Volchenkov G, Wagner D, van der Werf MJ, Williams B, Yew WW, Zellweger JP, Cirillo DMTBNET (2014) Management of patients with multidrug-resistant/extensively drug-resistant tuberculosis in Europe: a TBNET consensus statement. Eur Respir J 44(1):23–63. https://doi.org/10.1183/09031936.00188313

Languillon J (1971) The effects of thalidomide on leprosy reaction. Int J Lepr Other Mycobact Dis 39(2):590–592. http://ila.ilsl.br/pdfs/v39n2pt2a61.pdf. Accessed 04-02-2025

LeMagueres P, Im H, Dvorak A, Strych U, Benedik M, Krause KL (2003) Crystal structure at 1.45 A resolution of alanine racemase from a pathogenic bacterium, *Pseudomonas aeruginosa*, contains both internal and external aldimine forms. Biochemistry 42(50):14752–14761. https://doi.org/10.1021/bi030165v

LeMagueres P, Im H, Ebalunode J, Strych U, Benedik MJ, Briggs JM, Kohn H, Krause KL (2005) The 1.9 A crystal structure of alanine racemase from *Mycobacterium tuberculosis* contains a conserved entryway into the active site. Biochemistry 44(5):1471–1481. https://doi.org/10.1021/bi0486583

Liu CL, Lu YT, Tsai IF, Wu LC, Chien WC, Chung CH, Ma KH (2020) Fenofibrate facilitates post-active tuberculosis infection in macrophages and is associated with higher mortality in patients under long-term treatment. J Clin Med 9(2):337. https://doi.org/10.3390/jcm9020337

Liu JL, Liu XQ, Shi YW (2012) Expression, purification, and characterization of alanine racemase from *Pseudomonas putida* YZ-26. World J Microbiol Biotechnol 28(1):267–274. https://doi.org/10.1007/s11274-011-0816-1

Maitra A, Bates S, Shaik M, Evangelopoulos D, Abubakar I, McHugh TD, Lipman M, Bhakta S (2016) Repurposing drugs for treatment of tuberculosis: a role for non-steroidal anti-inflammatory drugs. Br Med Bull 118(1):138–148. https://doi.org/10.1093/bmb/ldw019

Mehta K, Khambete M, Abhyankar A, Omri A (2023) Anti-tuberculosis mur inhibitors: structural insights and the way ahead for development of novel agents. Pharmaceuticals (Basel, Switzerland) 16(3):377. https://doi.org/10.3390/ph16030377

Müller A, Klöckner A, Schneider T (2017) Targeting a cell wall biosynthesis hot spot. Nat Prod Rep 34:909–932. https://doi.org/10.1039/c7np00012j

Muniyandi M, Ramachandran R (2017) Current and developing therapies for the treatment of multi drug resistant tuberculosis (MDR-TB) in India. Expert Opin Pharmacother 18(13):1301–1309. https://doi.org/10.1080/14656566.2017.1365837

Muralikumar S, Vetrivel U, Narayanasamy A, Das UN (2017) Probing the intermolecular interactions of PPARγ-LBD with polyunsaturated fatty acids and their anti-inflammatory metabolites to infer most potential binding moieties. Lipids Health Dis 16(1):17. https://doi.org/10.1186/s12944-016-0404-3

Muthukumaran S, Sulochana KN, Umashankar V (2021) Structure based design of inhibitory peptides targeting ornithine decarboxylase dimeric interface and *in vitro* validation in human retinoblastoma Y79 cells. J Biomol Struct Dyn 39(14):5261–5275. https://doi.org/10.1080/07391102.2020.1785331

Nagarajan H, Deepika Lakshmi P, Vetrivel U (2020) Deciphering potential inhibitors targeting THI4 of *Fusarium solani* sp. to combat fungal keratitis: An integrative computational approach. Comput Biol Chem 88:107350. https://doi.org/10.1016/j.compbiolchem.2020.107350

Napier RJ, Rafi W, Cheruvu M, Powell KR, Zaunbrecher MA, Bornmann W, Salgame P, Shinnick TM, Kalman D (2011) Imatinib-sensitive tyrosine kinases regulate mycobacterial pathogenesis and represent therapeutic targets against tuberculosis. Cell Host Microbe 10(5):475–485. https://doi.org/10.1016/j.chom.2011.09.010

Noda M, Matoba Y, Kumagai T, Sugiyama M (2004) Structural evidence that alanine racemase from a D-cycloserine-producing microorganism exhibits resistance to its own product. J Biol Chem 279(44):46153–46161. https://doi.org/10.1074/jbc.M404605200

Ogasawara Y, Dairi T (2021) Discovery of an alternative pathway of peptidoglycan biosynthesis: a new target for pathway specific inhibitors. J Ind Microbiol Biotechnol 48(9–10):kuab038. https://doi.org/10.1093/jimb/kuab038

Olson GT, Fu M, Lau S, Rinehart KL, Silverman RB (1998) An aromatization mechanism ofinactivation of γ-aminobutyric acid aminotransferase for the antibiotic L-cycloserine. J Am Chem Soc 120(10):2256–2267. https://doi.org/10.1021/ja972907b

Pazos M, Peters K (2019) Peptidoglycan. Subcell Biochem 92:127–168. https://doi.org/10.1007/978-3-030-18768-2_5

Peisach D, Chipman DM, Van Ophem PW, Manning JM, Ringe D (1998) D-cycloserine inactivation of d-amino acid aminotransferase leads to a stable noncovalent protein complex with an aromatic cycloserine-PLP derivative. J Am Chem Soc 120:2268–2274. https://doi.org/10.1021/ja973353f

Perveen S, Kumari D, Singh K, Sharma R (2022) Tuberculosis drug discovery: progression and future interventions in the wake of emerging resistance. Eur J Med Chem 229:114066. https://doi.org/10.1016/j.ejmech.2021.114066

Petersen HG (1995) Accuracy and efficiency of the particle mesh Ewald method. Jchem Phys 103:3668–3679. https://doi.org/10.1063/1.470043

Raymond JB, Mahapatra S, Crick DC, Pavelka MS Jr (2005) Identification of the namH gene, encoding the hydroxylase responsible for the N-glycolylation of the mycobacterial peptidoglycan. J Biol Chem 280(1):326–333. https://doi.org/10.1074/jbc.M411006200

Rubinstein A, Major DT (2010) Understanding catalytic specificity in alanine racemase from quantum mechanical and molecular mechanical simulations of the arginine 219 mutant. Biochemistry 49(18):3957–3964. https://doi.org/10.1021/bi1002629

Ryckaert J-P, Ciccotti G (1977) Berendsen HJC (1977) Numerical integration of the cartesian equations of motion of a system with constraints: molecular dynamics of n-alkanes. J Comput Phys 23:327–341. https://doi.org/10.1016/0021-9991(77)90098-5

Sadhasivam A, Vetrivel U (2019) Identification of potential drugs targeting L, L-diaminopimelate aminotransferase of *Chlamydia trachomatis*: an integrative pharmacoinformatics approach. J Cell Biochem 120(2):2271–2288. https://doi.org/10.1002/jcb.27553

Sahrawat TR (2024) Role of artificial intelligence and machine learning in sustainable drug discovery. Braz Arch Biol Technol 67:e24240538. https://doi.org/10.1590/1678-4324-2024240538

Samdani A, Vetrivel U (2018) POAP: a GNU parallel based multi-threaded pipeline of open babel and AutoDock suite for boosted high throughput virtual screening. Comput Biol Chem 74:39–48. https://doi.org/10.1016/j.compbiolchem.2018.02.012

Santos LHS, Ferreira RS, Caffarena ER (2019) Integrating molecular docking and molecular dynamics simulations. Methods Mol Biol (Clifton, N.J.) 2053:13–34. https://doi.org/10.1007/978-1-4939-9752-7_2

Sathiyamani B, Daniel EA, Ansar S, Esakialraj BH, Hassan S, Revanasiddappa PD, Keshavamurthy A, Roy S, Vetrivel U, Hanna LE (2023) Structural analysis and molecular dynamics simulation studies of HIV-1 antisense protein predict its potential role in HIV replication and pathogenesis. Front Microbiol 14:1152206. https://doi.org/10.3389/fmicb.2023.1152206

Shaku M, Ealand C, Matlhabe O, Lala R, Kana BD (2020) Peptidoglycan biosynthesis and remodeling revisited. Adv Appl Microbiol 112:67–103. https://doi.org/10.1016/bs.aambs.2020.04.001

Shaw JP, Petsko GA, Ringe D (1997) Determination of the structure of alanine racemase from *Bacillus stearothermophilus* at 1.9-A resolution. Biochemistry 36(6):1329–1342. https://doi.org/10.1021/bi961856c

Singh G, Kumar A, Maan P, Kaur J (2017) Cell wall associated factors of mycobacterium tuberculosis as major virulence determinants: current perspectives in drugs discovery and design. Curr Drug Targets 18(16):1904–1918. https://doi.org/10.2174/1389450118666170711150034

Singh R, Dwivedi SP, Gaharwar US, Meena R, Rajamani P, Prasad T (2020) Recent updates on drug resistance in *Mycobacterium tuberculosis*. J Appl Microbiol 128(6):1547–1567. https://doi.org/10.1111/jam.14478

Sivashanmugam M, Sulochana KN, Umashankar V (2019) Virtual screening of natural inhibitors targeting ornithine decarboxylase with pharmacophore scaffolding of DFMO and validation by molecular dynamics simulation studies. J Biomol Struct Dyn 37(3):766–780. https://doi.org/10.1080/07391102.2018.1439772

Soda K, Tanizawa K (1990) Thermostable alanine racemase. Its structural stability. Ann N Y Acad Sci 585:386–393. https://doi.org/10.1111/j.1749-6632.1990.tb28071.x

Strych U, Penland RL, Jimenez M, Krause KL, Benedik MJ (2001) Characterization of the alanine racemases from two mycobacteria. FEMS Microbiol Lett 196(2):93–98. https://doi.org/10.1111/j.1574-6968.2001.tb10547.x

Theron G, Peter J, Richardson M, Barnard M, Donegan S, Warren R, Steingart KR, Dheda K (2014) The diagnostic accuracy of the GenoType(®) MTBDRsl assay for the detection of resistance to second-line anti-tuberculosis drugs. The Cochrane database of systematic reviews 10:CD010705. https://doi.org/10.1002/14651858.CD010705.pub2

Umashankar V, Deshpande SH, Hegde HV, Singh I, Chattopadhyay D (2021) Phytochemical moieties From Indian traditional medicine for targeting dual hotspots on SARS-CoV-2 spike protein: an integrative *in-silico* approach. Front Med 8:672629. https://doi.org/10.3389/fmed.2021.672629

Van Heijenoort J (2001) Recent advances in the formation of the bacterial peptidoglycan monomer unit. Nat Prod Rep 18(5):503–519. https://doi.org/10.1039/a804532a

Vasava MS, Bhoi MN, Rathwa SK, Borad MA, Nair SG, Patel HD (2017) Drug development against tuberculosis: past, present and future. Indian J Tuberc 64(4):252–275. https://doi.org/10.1016/j.ijtb.2017.03.002

Vivekanandan S, Vetrivel U, Hanna LE (2022) Design of human immunodeficiency virus-1 neutralizing peptides targeting CD4-binding site: an integrative computational biologics approach. Front Med 9:1036874. https://doi.org/10.3389/fmed.2022.1036874

Wang Z, Wang X, Li Y, Lei T, Wang E, Li D, Kang Y, Zhu F, Hou T (2019) farPPI: a webserver for accurate prediction of protein-ligand binding structures for small-molecule PPI inhibitors by MM/PB(GB)SA methods. Bioinformatics (Oxford, England) 35(10):1777–1779. https://doi.org/10.1093/bioinformatics/bty879

Wei Y, Qiu W, Zhou XD, Zheng X, Zhang KK, Wang SD, Li YQ, Cheng L, Li JY, Xu X, Li MY (2016) Alanine racemase is essential for the growth and interspecies competitiveness of *Streptococcus mutans*. Int J Oral Sci 8(4):231–238. https://doi.org/10.1038/ijos.2016.34

WHO (2024) https://www.who.int/teams/global-tuberculosis-programme/tb-reports. Accessed 04-02-2025

Wu X, Xu LY, Li EM, Dong G (2022) Application of molecular dynamics simulation in biomedicine. Chem Biol Drug des 99(5):789–800. https://doi.org/10.1111/cbdd.14038

Yan X, Gai Y, Liang L, Liu G, Tan H (2007) A gene encoding alanine racemase is involved in spore germination in *Bacillus thuringiensis*. Arch Microbiol 187(5):371–378. https://doi.org/10.1007/s00203-006-0201-x

Yang S, Xu Y, Wang Y, Ren F, Li S, Ding W, Ma Y, Zhang W (2018) The biological properties and potential interacting proteins of d-Alanyl-d-alanine ligase a from *Mycobacterium tuberculosis*. Molecules (Basel, Switzerland) 23(2):324. https://doi.org/10.3390/molecules23020324

Publisher's Note Springer Nature remains neutral with regard to jurisdictional claims in published maps and institutional affiliations.

Springer Nature or its licensor (e.g. a society or other partner) holds exclusive rights to this article under a publishing agreement with the author(s) or other rightsholder(s); author self-archiving of the accepted manuscript version of this article is solely governed by the terms of such publishing agreement and applicable law.